ARTICLE

This is the accepted version of the following article: J. Mater. Chem. A*, 2021,9, 301-309, *which has been published in final form at
https://doi.org/10.1039/D0TA08452B

Received 00th January 20xx,
Accepted 00th January 20xx

DOI: 10.1039/x0xx00000x

Fluorene-based enamines as low-cost and dopant-free hole transporting materials for high performance and stable perovskite solar cells

Sarune Daskeviciute,[†a] Cristina Momblona,[†b] Kasparas Rakstys,[a] Albertus Adrian Sutanto,[b] Maryte Daskeviciene,[a] Vygintas Jankauskas,[c] Alytis Gruodis,[c] Giedre Bubniene,[a] Vytautas Getautis,*[a] Mohammad Khaja Nazeeruddin*[b]

The power conversion efficiency of perovskite solar cells is approaching the Shockley-Queisser limit, therefore this technology is next to the commercialization stage. The inexpensive and stable hole transporting materials are highly desirable towards the successful scale-up. Most high performing devices generally employ expensive hole conductors that are synthesized via cross-coupling reactions that require expensive catalysts, inert reaction conditions and time-consuming sophisticated product purification. In a quest to employ cost-effective chemistry to combine the building blocks, we explore enamine-based small molecules that can be synthesized in a simple condensation reaction from commercially available materials leading to an estimated material cost of few euros per gram. Synthesized fluorene-based enamines exhibit very high hole mobility up to 3.3×10^{-4} cm^2/Vs and enables the fabrication of perovskite solar cells with a maximum power conversion efficiency of 19.3% in doped configuration and 17.1% without doping. In addition, both PSCs systems demonstrate superior long-term stability compared to spiro-OMeTAD. This work shows that hole transporting materials prepared via simple condensation protocol have the potential to compete in performance with materials obtained via expensive cross-coupling methods at a fraction of their cost and deliver exceptional stability of the final device. This work provides a design strategy for the further development of novel, low-cost semiconductors.

Introduction

During its first-decade hybrid organic-inorganic halide perovskite-based solar cells (PSCs) have continually improved. They are now approaching the Shockley-Queisser power conversion efficiency (PCE) limit with the current best certified PCE of 25.5%.[1] The improvement in PCE can be attributed to the outstanding optoelectronic properties as high absorption coefficient, long carrier diffusion length, small exciton binding energy, and high charge carrier mobility of the perovskite material and rapid advances in the device engineering.[2–6] In combination with highly abundant precursor materials and simple preparation methods it is believed that the commercialization of PSC technology during the second decade is inevitable.[7–9]

While the very high efficiency using perovskites is a significant achievement, issues relating to the high price of device components such as hole transporting material (HTM) and long-term stability against moisture, heat, and light are still a concern for commercial application of the technology, therefore breaking these bottlenecks is a must for the realization of cost-effective and stable devices.[10–14]

Until now, most of the highly efficient PSCs are based on either the small organic molecule 2,2',7,7'- tetrakis(*N*,*N*-di-*p*-methoxyphenylamine)-9,9'-spirobifluorene (spiro-OMeTAD) or conjugated macromolecule poly[bis(4-phenyl)(2,4,6-trimethylphenyl)amine] (PTAA) HTMs, both of which are very expensive.[14–17] For example, spiro-OMeTAD is synthesized in multi-step reaction scheme that requires low temperature (-78°C), sensitive (*n*-butyllithium) and aggressive (Br_2) reagents resulting in a relative high material cost, consequently leading to a significant contribution to the total device cost.[18–20]

[a] *Department of Organic Chemistry, Kaunas University of Technology, Radvilenu pl. 19, Kaunas 50254, Lithuania.*
[b] *Group for Molecular Engineering of Functional Material, Institute of Chemical Sciences and Engineering, École Polytechnique Fédérale de Lausanne, CH-1951 Sion, Switzerland.*
[c] *Institute of Chemical Physics, Vilnius University, Sauletekio al. 3, Vilnius 10257, Lithuania.*
† These authors contributed equally to this work.
Electronic Supplementary Information (ESI) available: [details of any supplementary information available should be included here]. See DOI: 10.1039/x0xx00000x

Additionally, the tedious synthesis hampers large scale production and thereby could impede the commercial success of PSCs.

Therefore, huge interest of many research groups has been directed into new HTM candidates to find an ideal HTM, which would be easily scalable for reasonable cost including spiroxanthene-,[21–23] fluorene-,[24,25] carbazole-,[26–31] silane-,[32] bifluorene-,[33] pyrene-,[34,35] and bifluorenylidene-based[36] examples. However, most of conjugated HTMs are generally designed by linking together building blocks of conjugated central core with costly diphenylamine or triphenylamine containing methoxy-substituted side groups using C–N or C–C cross-coupling chemistry, respectively. These coupling reactions generally require stringent reaction conditions resulting in several disadvantages, such as inert reaction conditions, expensive transition metal catalysts and extensive purification procedures. The commonly used purification methods involve sublimation or repeated column chromatography due to the inherent formation of side products that are prone for this type of reactions and tiny amount metal catalyst residues that may remain in the hole transporting layer. The metal catalyst residues act as traps that deteriorate the charge-transporting properties of the synthesized HTMs and negatively affect the performance of the resulting devices as well as greatly reduce the material yield and therefore further increase the final product costs. Alongside the high processing cost in turn results in a significant cost contribution of HTMs, making them industrially less interesting.

To this extent, significant effort is now being put towards finding the simplified synthetic protocols in order to reduce the cost of HTM synthesis without sacrificing the efficiency. Recently, several research groups have focussed on tuning the structure by decreasing the number of synthetic steps, thus reducing the synthetic complexity, cost of materials and the environmental impact.[37,38] This includes reports based on azomethine,[39] hydrazone,[40] amide[41] by Petrus et al and our previously explored aniline[42] and carbazole[43,44] enamines prepared by facile condensation reaction. In this sense, condensation chemistry is an excellent perspective moving away from palladium-catalysed reactions since water is the only side-product and expensive catalysts are not required. Moreover, simple product workup and purification drastically reduce the cost of the final product.

In this work, we further explore the potential of enamine family HTMs employing fluorene as the central scaffold. Five different substituents containing fluorene-based HTMs were successfully synthesised employing facile synthesis using commercially available and cheap reagents. Their optical, thermal, electrophysical, and photovoltaic properties were thoroughly investigated by combining the experimental and simulation methods. Moreover, the impact of differently substituted central fluorene core on different properties of synthesized molecules, in comparison to our earlier reports, have been systematically investigated. All these enamine-based HTMs have been successfully applied in PSCs with and without additives showing a photovoltaic performance of up to 19.3% and 17.1%, respectively, with excellent long-term stability in both cases. With this we demonstrate that both simple chemistry and product purification result in estimated material costs of a few euros per gram without sacrificing the efficiency and in contrary enhancing the stability.

Results and discussion

Fluorene enamines were synthesized using straightforward chemistry with excellent yields and high purity. As shown in **Figure 1**, **V1275** only required one-pot reaction condensing inexpensive commercially available reagents 2,7-diaminofluorene and 2,2-bis(4-methoxyphenyl)acetaldehyde in the presence of camphor sulfonic acid. The reaction is performed under ambient conditions and water is the only by-product separated from the reaction mixture using a Dean–Stark trap accelerating the formation of the final product and significantly reducing the reaction duration. Moreover, we note that column chromatography or vacuum sublimation processes are avoided for the purification and the simplicity of the condensation chemistry reduces batch-to-batch variations.

V1275 was further reacted with different alkylating agents to yield methyl-, propyl-, hexyl-, and benzyl-substituted fluorene enamines as final HTMs **V1237**, **V1235**, **V1236**, and **V1227**, respectively. The chemical structures of the synthesized products were verified by NMR spectroscopy, and elemental analysis. Detailed synthetic procedures and analysis are reported in the SI. In order to assess the price of synthesized materials, we performed a cost-analysis on a lab scale synthesis (**Table S1**).[45] The estimated cost of **V1275** is ~10 €/g and around 22 €/g for alkylated product **V1235**, which are the fraction of cost of spiro-OMeTAD (~92€/g)[46] and less than that of our previously developed double-armed carbazole enamines mainly due to the less expensive 2,7-diaminofluorene starting reagent.[44]

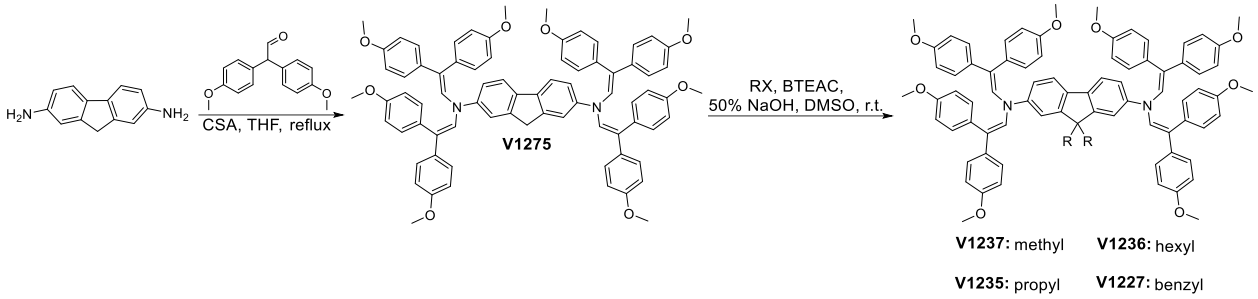

Figure 1. Straightforward reaction scheme of fluorene enamine HTMs and their molecular structures.

Quantum chemical calculations were performed with Gaussian09 software to establish the most probable molecular geometry and absorption spectrum.[47] Density functional theory (DFT) method B3LYP/6-31G was used for geometry optimization. **V1275**, **V1237**, and **V1227** have been chosen as a model compounds for computations as the different length of aliphatic substituents should not affect the electronic properties and was ignored. Due to fragmental motions, big number of different conformers could be formed. Only two typical and most probable conformers of each compound (a and b, after ground state geometry optimization) are presented in **Figures S1-3**. Conformers could be formed due to following condition: enamino subfragments are formed as quite well expressed π-conjugated fragments >C=CH–N*–CH=C< oriented quasi linearly, and this bridge between two O-Ph subsubfragments must be treated as the important factor for fragment displacement in space. Two chains of O-Ph subfragments of left and right fragments could be oriented in the shape of the upper-side roof according to fluorene core (see **V1237**, **V1275** a and b, bottom part), but another O-Ph subfragments are oriented chaotically (see **V1227**, a and b, top part). Due to the presence of benzyl substituents in **V1227**, it is necessary to conclude that phenyl fragments are not included in core π-conjugated system (connection through two single –C–C– bonds of the big lability). Possibility to orient the phenyl on fluorene core could be realized in many ways. This factor of indeterminacy of phenyl position creates the condition of non-ordered distribution of enamino subfragments in **V1227** structure. For all three derivatives, b conformers are more ordered in comparison to a. Semiempirical TD method (for singlets only) was used for simulation of the electronic absorption spectrum. **Table S2** represents the excitation parameters for three lowest excited states S_1, S_2, S_3: transition energy and oscillator strength. For all compounds (including both conformers), $S_0 \rightarrow S_1$ transitions are allowed and partially allowed (oscillator strength in interval 0.57-0.71) and transition energy approximately 2.89-2.92 eV. **Table S3** represents the scheme of the population of excited electronic states and the corresponding set of MO.

Distributions of electron density for the HOMO-1, HOMO as well as the LUMO and LUMO+1 for **V1275**, **V1237**, and **V1227** structures, are presented in **Figures S4-6**. Any pure CT charge redistribution behaviour was established for both, a and b conformers, only charge redistribution between first and second amino subfragment of left enamino fragment takes place. It is necessary to point out that amino subfragments could play the role of charge donors as well as charge acceptors, depending on fragment orientation to the central core fluorene unit (a conformer, HOMO→LUMO transition). Also, charge redistributions between the enamino fragment and fluorene core takes place (b conformer, HOMO→LUMO transition and a conformer, HOMO→LUMO+1 transition). In general, charge redistribution between left and right enamino substituents and central core fluorene unit is typical for both conformers.

The thermal behaviour of HTMs was evaluated by thermogravimetric analysis (TGA) (**Figure 2a**) and differential scanning calorimetry (DSC) (**Figure S7**) techniques. TGA analysis has shown that **V1275** has the highest thermal stability among the series with decomposition temperature (T_{dec}) of 403°C at 5% weight loss. The introduction of the aliphatic substituents to the central fluorene position has led to the deteriorated thermal resistance. However, we note that instant weight loss at around 400°C is observed for all new materials suggesting that they may undergo sublimation rather than decomposition, enabling them to be vacuum-deposited. The thermal transitions of V-series molecules were determined by DSC. Interestingly, it was found that **V1275**, **V1236**, and **V1227** exist both in the crystalline and the amorphous state while **V1237** and **V1235** tend to crystallize. Only the glass transition temperature (T_g) was investigated for all compounds during the second heating scan, while **V1237** has the most stabilized amorphous state with the glass transition detected at 153°C.

The UV–Visible absorption and photoluminescence (PL) spectra of the synthesized HTMs in THF solutions and solid films are depicted in **Figure 2b** and **Figure S8**, respectively. All HTMs have two major absorption peaks at approximately 260 nm and 400 nm. The less intense absorption peak at shorter wavelength corresponds to localised π–π* transitions. Longer wavelength arises from more intensive delocalisation from the conjugated scaffold and is assigned to n–π* transitions. Change of the different aliphatic fragments has not influenced the conjugation, therefore, spectra of all molecules are almost identical, however, there is a significant difference in the absorption intensity ratio of **V1227** peaks arising from benzyl moieties. The PL spectra of all compounds are similar with the peak at 510 nm, showing that significantly large Stokes shifts of approximately 100 nm are observed for all molecules, therefore significant changes in the geometry of the molecules are desired upon excitation. The optical gaps (E_g) of HTMs were

calculated from the intersection of absorption and PL spectra of thin films and were found to be identical for all the materials at around 2.8 eV.

To understand the energy level alignment of the HTMs in PSCs, we next measured solid-state ionization potential (I_P) using the electron photoemission in the air of the thin films (PESA) with the experimental data shown in **Figure 2c**. **V1275**, **V1237**, **V1235**, **V1236**, and **V1227** were found to have I_P values of 5.01, 5.0, 5.03, 5.03 and 4.9 eV, respectively, which ideally align with the valence band (VB) energy of the triple cation-based perovskite (~5.70 eV), therefore efficient hole transfer from perovskite to the cathode should be ensured.[48] Spiro-OMeTAD has been measured as well and was found to have a very similar ionization potential of 5.00 eV (**Figure S9**). Additionally, to reveal the effect of p-doping as electron acceptor we have evaluated the ionization potentials of doped layers (I_P*) since it is known to control the HOMO energy level by removing electrons from the HOMO to generate holes of an intrinsic HTM enhancing the device efficiency.[14,49–51] HTMs were doped using the same manner as in the device fabrication part detailed in the SI. As expected, upon doping ionization potentials were stabilized by around 0.3 eV further reducing the overpotential with the VB of perovskite thus expectedly increasing the V_{OC} in doped HTL containing devices including spiro-OMeTAD (**Figure S10-S11**). Based on the solid-state optical gap and I_P values we calculated the electron affinities (E_{ea}) of the enamine materials to be 2.22, 2.21, 2.22, 2.24, and 2.11 eV for **V1275**, **V1237**, **V1235**, **V1236**, and **V1227**, respectively. Importantly, the electron affinities of the compounds are smaller than the conduction band energy of the perovskite (-4.10 eV), and therefore they should effectively block electron transfer from the perovskite to the anode.[48] We next measured the charge mobility of the V-series using the xerographic time of flight (XTOF) technique. Dependences of hole drift mobility on electric field strength are depicted in **Figure 2d**. Zero-field hole drift mobility (μ_0) for **V1275**, **V1237**, **V1235**, and **V1236** were determined to be at 10^{-4} cm^2/Vs, while propyl-substituted **V1235** was found to have the highest hole mobility of 3.3×10^{-4} cm^2/Vs among the series. We note that this is also the highest hole mobility comparing with our previous aniline and carbazole enamine reports and outperforms that of spiro-OMeTAD (μ_0 = 1.3×10^{-4} cm^2/Vs).[36,44] Switching to the aromatic benzyl substitution has negatively influenced the hole drift mobility as **V1227** showed the lowest result of 8×10^{-5} cm^2/Vs due to the larger energetic disorder. The thermal, optical, and photoelectrical properties of the novel HTMs are listed in **Table 1**.

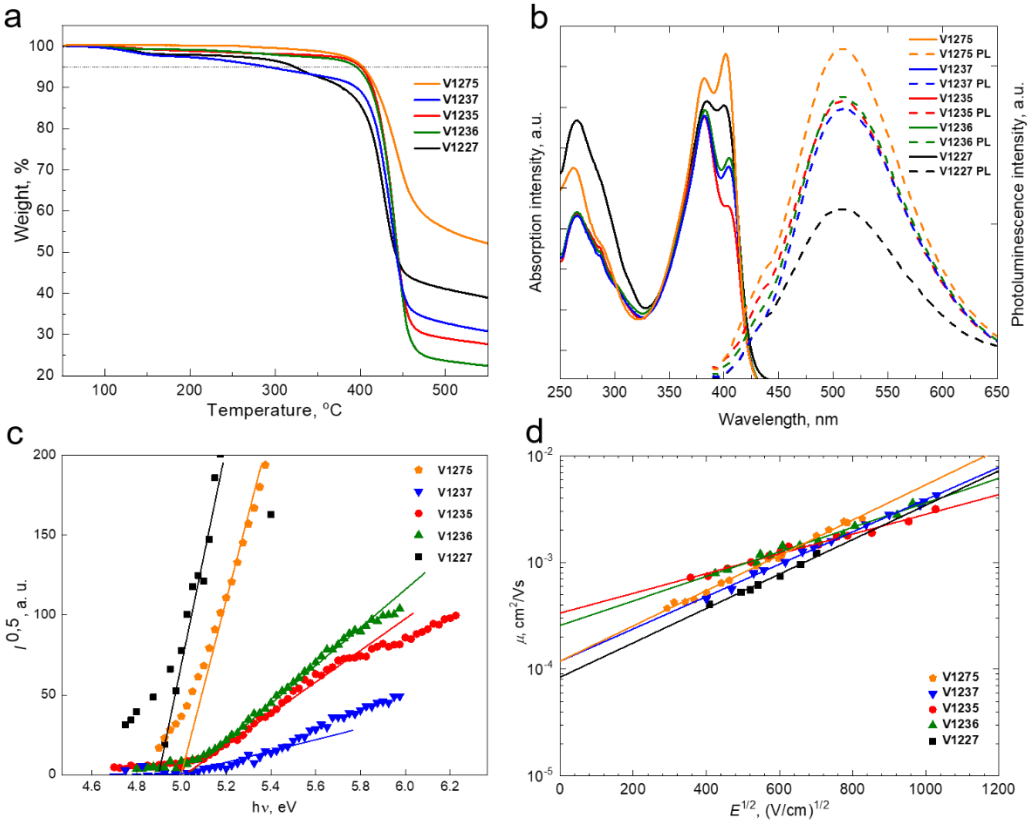

Figure 2. a) Thermogravimetric analysis (TGA) data (heating rate of 10 °C/min, N_2 atmosphere); b) UV–Vis absorption (solid line) and photoluminescence (dashed line) spectra of V-series HTMs in THF solutions (10^{-4} M); c) Photoemission in air spectra of the charge transporting layers **V1275**, **V1237**, **V1235**, **V1236**, and **V1227**; d) Electric field dependencies of the hole-drift mobility in synthesized HTMs.

Table 1. Thermal, optical and photophysical properties of newly synthesized enamines.

ID	T_m (°C)[a]	T_c (°C)[a]	T_g (°C)[a]	T_{dec} (°C)[a]	λ_{abs} (nm)[b]	λ_{em} (nm)[b]	I_P (eV)[c]	I_P* (eV)[d]	E_g (eV)[e]	E_{ea} (eV)[f]	μ_0 ($cm^2 V^{-1} s^{-1}$)[g]
V1275	255	-	150	403	262, 381, 401	508	5.01	5.39	2.79	2.22	$1.2 \cdot 10^{-4}$
V1237	247, 267, 272	198	153	285	265, 382, 404	510	5.0	5.32	2.79	2.21	$1.2 \cdot 10^{-4}$
V1235	273	159	120	399	266, 382, 404	509	5.03	5.39	2.81	2.22	$3.3 \cdot 10^{-4}$
V1236	173, 195	-	90	393	265, 383, 404	508	5.03	5.25	2.79	2.24	$2.6 \cdot 10^{-4}$
V1227	330	-	116	321	265, 384, 400	507	4.9	5.34	2.79	2.11	$8 \cdot 10^{-5}$

[a]Melting (T_m), crystallization (T_c), glass transition (T_g) and decomposition (T_{dec}) temperatures observed from DSC and TGA, respectively (10 °C/min, N_2 atmosphere); [b]Absorption and emission (excitation = $\lambda_{abs\ max}$) spectra were measured in THF solutions (10^{-4} M); [c]Ionization energies of the films measured using PESA without and [d]with doping; [e]E_g estimated from the intersection of absorption and emission spectra of solid films; [f]$E_{ea} = I_P - E_g$; [g]Mobility value at zero field strength.

The new V-series HTMs was implemented into *n-i-p* solar cells with the layout: fluorine-doped tin oxide (FTO)/compact TiO_2 (c-TiO_2)/mesoporous TiO_2 (m-TiO_2)/SnO_2/perovskite/HTM/Au, where the HTMs were doped with *tert*-butylpyridine (tBP), tris(bis(trifluoromethylsulfonyl)imide) (LiTFSI) and tris(2-(1*H*-pyrazol-1-yl)-4-*tert*-butylpyridine)cobalt(III) (FK209). The detailed fabrication procedure can be found in the SI.

Cross-sectional scanning electron microscope (SEM) imaging was performed on the complete devices fabricated with the V-series and spiro-OMeTAD (**Figure 3a** and **Figure S12-S13**). The analysis of the images denotes that the HTM layers are compact and uniform on top of the perovskite layer with thickness of ~150 nm for **V1275**, **V1237**, **V1235** and **V1236**, ~120 nm for **V1227**, and ~260 nm for spiro-OMeTAD. The HTM thickness of the dopant-free devices were extracted from its respective cross-sectional SEM images (**Figure S13**), obtaining films of ~70 nm. To shed light on the dopant-free and doped-HTM layers, surface morphology scanning electron microscopy was performed (**Figure S14** and **Figure S15**). All the HTMs layers were deposited on top of FTO-glass with the same depositing conditions than in the device fabrication. All the images of doped-HTM thin films show homogeneous and complete surface coverage without the presence of material aggregation.[52] Similar morphology was observed for the dopant-free HTM layers but due to the thinner layer thickness than in the doped counterparts, the layer underneath can be intuited. The energy levels of the complete devices with the studied HTMs as well as spiro-OMeTAD can be found in **Figure 3b**.[48,53] The current density – voltage (*J–V*) curves of the best-performing devices fabricated with V-series HTMs and spiro-OMeTAD are compared and presented in **Figure 3c**. The corresponding photovoltaic parameters were extracted and presented in **Table 2**. The devices containing **V1275**, alkylated-HTMs **V1237**, **V1235**, **V1236**, and spiro-OMeTAD present comparable photovoltaic behaviour with PCE around 19%. The comparison of the best-performing devices is confirmed by statistical data (**Figure S16**). The performance is greater than the benzyl-substituted **V1227**-based device with 12.5%. Note that, this trend can be related to the hole mobility values obtained for the HTMs, ranging from 1.2×10^{-4} cm^2/Vs to 3.3×10^{-4} cm^2/Vs for **V1275**, **V1235**, and similar to spiro-OMeTAD (1.3×10^{-4} cm^2/Vs), but lower for the bulky analogue **V1227** with hole mobility value of 8×10^{-5} cm^2/Vs.[44]

The photovoltaic characteristics (**Table 2**) show that the **V1275** and alkyl-based devices have almost identical short-circuit current density values (J_{SC}) in the range from 23.24 mA cm^{-2} for **V1275** to 22.86 mA cm^{-2} for **V1235**, respectively. This suggests that the substitution with an alkyl chain and the increasing alkyl chain length from methyl to hexyl do not strongly influence the charge collection properties of the perovskite layer. However, the benzyl-based **V1227** results in devices having a slightly lower J_{SC} value of 22.32 mA cm^{-2}. Such behaviour is also confirmed by the external quantum efficiency (EQE) spectra (**Figure S17a**). The corresponding integrated current densities from the respective EQEs (**Figure S17**) are presented in **Table 2** in brackets and the values are in good agreement with the measured values from the *J-V* characteristics (within 5% error). Similar fill-factor (FF) values are obtained for the device employing **V1275**, **V1237**, **V1235** and **V1236** with values ranging between 0.76 and 0.77. However, the FF in the device with **V1227** is reduced to 0.55, this can be explained by the presence of benzyl groups in **V1227**, which causes a less ordered packing of the molecules in the film and in the interface with perovskite, and this also leads to a greater dispersion of solar cell parameters (**Figure S16**) and a reduction in the FF.[54] The main parameter leading to the slightly lower performance of the V-series in comparison to spiro-OMeTAD corresponds to the open-circuit voltage (V_{OC}). The cells incorporating **V1275**, **V1237**, **V1235** and **V1236** exhibit lower values of V_{OC} (1077, 1090, 1089 and 1094 mV, respectively) than the reference device containing spiro-OMeTAD (1115 mV).

The series resistance (R_S) of the devices was calculated from the corresponding *J-V* curves. The R_S is reduced with the incorporation of dopants in the HTM layer due to the increase of the hole mobility in the layer.[55,56] The lowest series resistance values of 5.9, 6.2, 5.1 and 5.2 Ω are obtained for devices made with doped-**V1275**, **V1237**, **V1235** and **V1236** HTMs and are comparable to the value registered for the spiro-OMeTAD device (5.7 Ω). The series resistance in the doped **V1227**-based device is similar to the values obtained in the dopant-free series, denoting a charge carrier transport issue in the device. The presence of bulky benzyl group can induced to a less ordered packing of the molecules in the film, also confirmed by

DFT calculations, hence originating a possible poor charge transfer between the perovskite and the doped **V1227** layer. This interface issue might reduce the transport of charge carriers through the perovskite/HTM interface ultimately limiting the overwhole solar cell performance.[57]

On other hand, devices containing the dopant-free HTMs suffer from 4-5 times higher resistance than the doped-counterparts. The dopant-free HTM layer present higher resistance values even we tried to reduce the series resistance by lowering the HTM solution concentration from 20 mM for doped-HTM to 15 mM for dopant-free HTM to generate a thinner HTM layer. These higher values are reflected in the lower device performance for dopant-free HTMs. The use of the longer alkyl chain for the devices containing dopant-free HTMs increases the series resistance of the device. This suggest less ordered packing of the molecules in the film reducing the carrier transport through the perovskite/HTM interface and therefore HTM layer itself. This trend is not observed for the doped-HTMs counterparts.[57]

In order to evaluate the photogenerated hole extraction efficiency of the new HTMs, we performed thin-film steady-state PL measurements. Perovskite layers were deposited on top of glass and the PL spectra of the films were recorded under 625 nm excitation wavelength. Afterwards, the HTMs were deposited on top of the pristine perovskite layers with the same conditions than in the device fabrication. The quenching effect was analysed in comparison with the corresponding pristine perovskite layer and it is presented in **Figure 3d** and the percentage of PL quenching for each HTM is showed in **Table S5**. In spite of the perovskite/HTM energy level mismatch, the decrease of PL intensity suggests a good hole-extraction capability and confirms the efficient extraction of holes across the interface from the VB of perovskite into the HOMO of enamine-based HTMs attributed to good perovskite/HTM contact.[58]

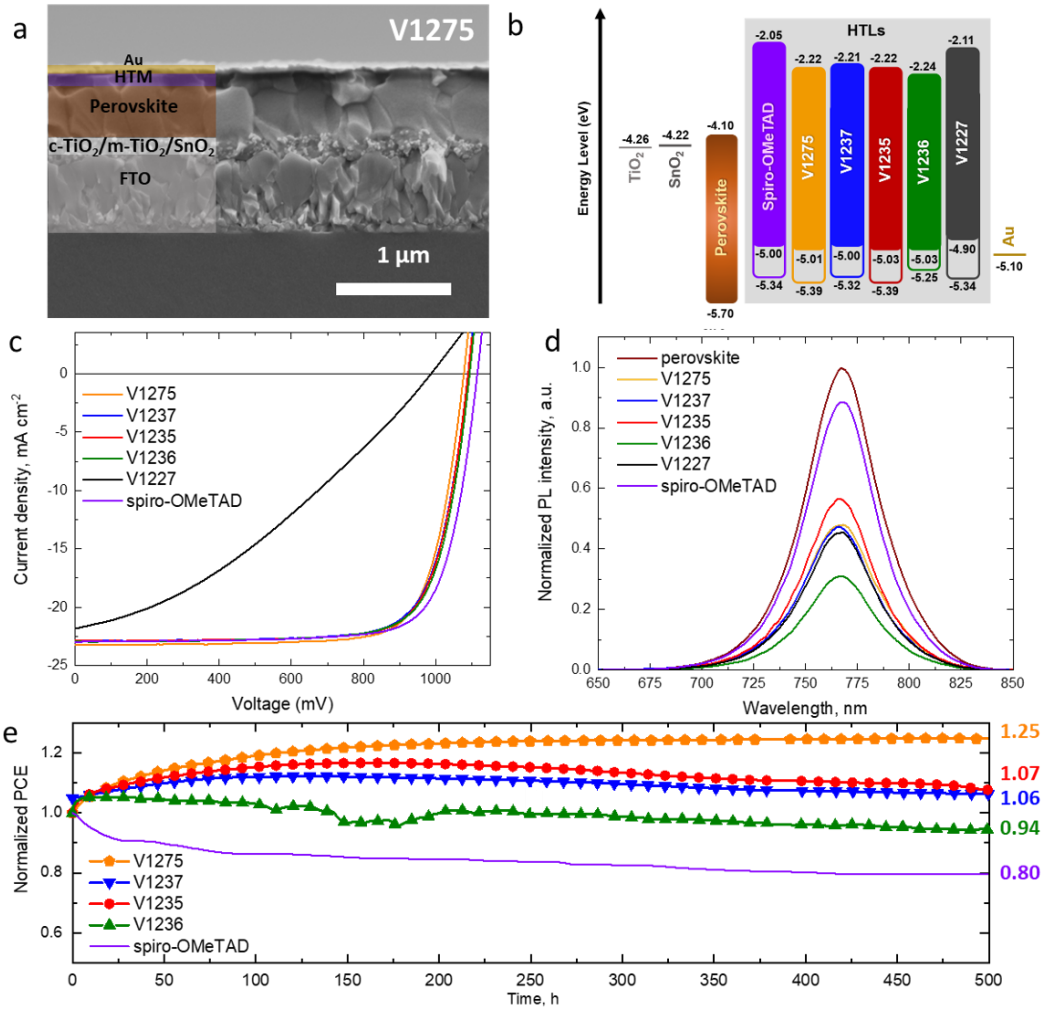

Figure 3. a) Cross-sectional SEM image of the photovoltaic device fabricated with doped **V1275** HTM; b) Schematic energy level diagram of the device representing the HOMO/LUMO and the stabilized HOMO of doped layers; c) *J – V* curves recorded for the champion devices for each doped HTM; d) Normalized steady-state photoluminescence spectra of perovskite and perovskite/HTM layers deposited on glass (λ_{exc}=625nm); e) Stability test of unencapsulated devices under continuous 1 sun illumination.

Table 2. Photovoltaic parameters, series resistance, and thickness of the fluorene-based enamines HTMs extracted from the best-performing devices. (Short-circuit current density calculated from the corresponding EQE).

	HTM	V_{OC} (mV)	J_{SC} (mA cm^{-2})	FF	PCE (%)	R_S (Ω)	HTM thickness (nm)
Doped-HTM	**V1275**	1077	23.24 (23.11)	0.77	19.3	5.9	~150
	V1237	1090	22.97 (22.74)	0.76	19.2	6.2	~150
	V1235	1089	22.86 (22.85)	0.77	19.2	5.1	~150
	V1236	1094	22.95 (22.94)	0.76	19.1	5.2	~150
	V1227	1024	22.32 (21.82)	0.55	12.6	26.0	~120
	spiro-OMeTAD	1115	22.97 (21.86)	0.77	19.7	5.7	~260
Dopant-free HTM	**V1275**	1033	22.95 (22.81)	0.72	17.1	22.2	~70
	V1237	1038	22.98 (22.93)	0.71	16.9	22.9	~70
	V1235	1029	23.09 (22.81)	0.70	16.6	24.5	~70
	V1236	1022	23.02 (22.88)	0.69	16.2	25.2	~70
	spiro-OMeTAD[59]	972	22.83	0.47	10.4		

The device stability was evaluated for the solar cells containing **V1275** and the alkyl-substituted HTMs (**V1237**, **V1235** and **V1236**) due to their higher efficiency in comparison with the benzyl-substituted HTM **V1227**. As a reference, the long-term stability of the spiro-OMeTAD-based device was also evaluated. All the devices were unencapsulated and kept under constant 1 sun illumination in N_2 atmosphere for 500 hours. The results of the long-term stability of the devices are presented in **Figure 3e**. For comparison, the study was carried out with all the devices kept under the same light source. The device containing the non-substituted **V1275** HTM shows a continuous rising of PCE achieving 125% of its original efficiency after 500 h under operation, being not only the highest thermally stable HTM of the series but also the most stable device under constant light illumination among them. The introduction of the methyl and propyl group (**V1237** and **V1235**) reduces this increase obtaining 107 and 106% of its original efficiency after 500 h. However, the PCE of the device containing the longest insulating hexyl chain **V1236** of the series is only reduced to 94% of its initial efficiency after 500 h under illumination.

Interestingly, although the length of the alkyl chains only slightly influences on the device performance, but it displays an influence on the long-term device stability. Even all the devices present exceptional long-term stability under light illumination, the introduction of an alkyl group and with longer alkyl chain trending to slightly deteriorated long-term light stability. Such behaviour may suggest that the degradation of the layer is enhanced with the lower degree of packing due to the longer insulating chains. The outstanding light stability of the doped V-series HTMs raised when compared with the most widely used HTM in PSC, spiro-OMeTAD, which efficiency is reduced to 80% from its initial performance after 500 h under constant illumination. With this result we can confirm that the use of dopants does not negatively affect in the long-term stability of PSCs, and this fact contradicts previously reported studies.[14]

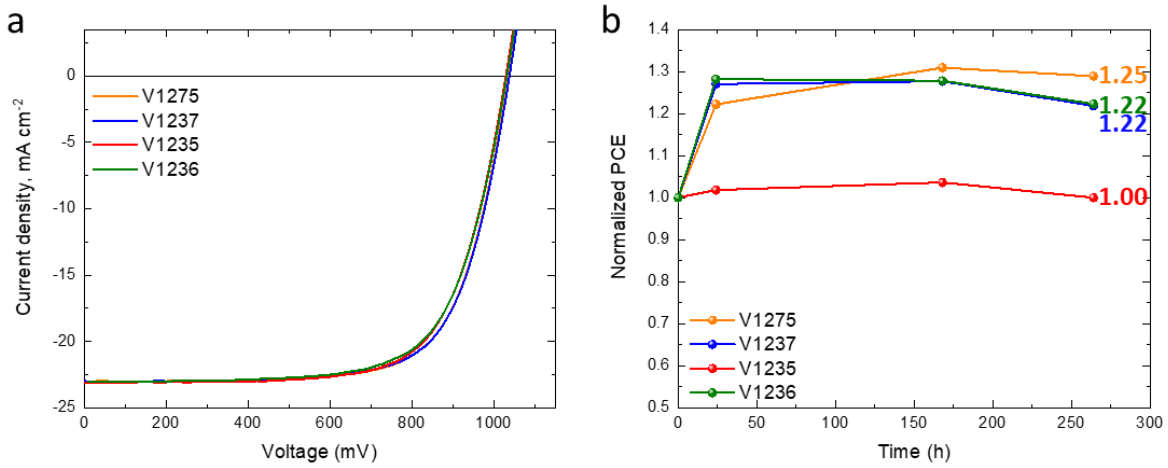

Figure 4. a) *J–V* curves recorded for the champion devices for each dopant-free HTM; b) shelf lifetime of unencapsulated devices fabricated with each dopant-free HTM (stored in dark and dry environment with RH<10%).

In order to evaluate if the dopants chemically interact with the HTMs and detrimentally affect the long-term stability of the devices, the most promising HTMs from the series, **V1275**, **V1237**, **V1235** and **V1236** were studied without the use of additives.[60–62] All of them showed efficiencies exceeding 16% (**Figure 4a** and **Table 2**) with improved device performance compared with the reported 10.39% PCE for dopant-free spiro-OMeTAD-based devices previously reported by our group (**Table 2**).[59] The initial *J-V* curves and its corresponding photovoltaic parameters are presented in **Figure S18** and Table S4. The corresponding EQEs and the integrated short-circuit current density are presented in **Figure S17b** and its values in **Table 2**. The statistical data (**Figure S19**) shows that the gradual increase of length of the alkyl substituents results in a slight deterioration in the device performance. Devices fabricated with non-alkylated HTM **V1275** are the highest efficient of the series, whereas the efficiency is gradually reduced by the introduction of the methyl, propyl, and hexyl groups **V1237**, **V1235** and **V1236**, respectively, mainly due to lower V_{OC} and *FF* values. This difference can be attributed to different packing of the molecules compared to the equivalent doped devices.

While the J_{SC} is similar to the equivalent doped devices, the V_{OC} and FF values are significantly lower. The higher resistance of the dopant-free HTM layer reduces the hole extraction and increases the interfacial recombination at the perovskite/HTM contact reflected in the drop of *FF* and V_{OC} in all the devices.[63] The stability of the dopant-free devices was performed by storing non-encapsulated devices in dark under dry air (RH<10%) and periodically tested under a relative humidity of 45% (**Figure 4b**). The PCE of all HTMs shows no degradation after 250 h from its fabrication. After 250 h, the device efficiency increases to reach 125%, 122%, 100%, 122% from its initial device efficiency for the **V1275**, **V1237**, **V1235** and **V1236** HTMs, respectively. This result demonstrates that V-series HTMs can also efficiently work as dopant-free HTMs in PSCs with excellent stability.

Conclusions

We report the synthesis, and a systematic study of the fluorene-based hole transporting enamines. Novel HTMs are easily attainable by a straightforward synthetic scheme ensuring cost-effective upscaling; in particular, **V1275** only required one-pot reaction condensing inexpensive commercially available reagents leading to the extremely low synthetic cost of approximately 10 €/g. The impact on different substitution in the central fluorene was revealed through the optical, electrochemical, photophysical, and photovoltaic measurements. PSCs using the V-series compounds were fabricated in doped- and dopant-free configuration. Synthesized materials exhibit very high hole mobility up to 3.3×10^{-4} cm^2/Vs leading to a light-to-energy power conversion efficiency exceeding 19% with the doped non-functionalized **V1275**, which is on par with the widely researched spiro-OMeTAD, with a remarkable improvement in the long-term stability. While the efficiency of the spiro-based device dropped up to 80% of the original PCE after 500 h without encapsulation and constant light illumination, the doped V-based devices achieved up to 125% of the original PCE in the same ageing time. The devices fabricated with dopant-free HTMs showed high efficiencies, exceeding 17%, with also excellent shelf-lifetime stability. The results presented here show that HTMs prepared via simple condensation protocol can compete in performance with materials obtained via expensive cross-coupling methods at a fraction of their cost and may be very attractive low-cost and stable semiconductors solving one of the concerns for the near future commercialization.

Conflicts of interest

There are no conflicts to declare.

Acknowledgements

This project has received funding from the European Union's Horizon 2020 research and innovation programme under the Marie Skłodowska–Curie grant agreement No 754462. We acknowledge the Swiss National Science Foundation (SNSF) funding through the Synergia Grant EPISODE (Grant No. CRSII5_171000). The authors (M. Daskeviciene and G. Bubniene) acknowledge funding from Research Council of Lithuania (grant No. MIP-19-14). Computations were performed on resources at the High Performance Computing Center „HPC Sauletekis" (Faculty of Physics, Vilnius University). Prof. R. Buonsanti is acknowledged for the use of the Fluorolog system and Dr. E. Kamarauskas is acknowledged for ionisation potential measurements. KR acknowledges the funding received from MJJ Foundation.

Notes and references

1 NREL, Photovoltaic Research: Best Research Cell Efficiency Chart, https://www.nrel.gov/pv/cell-efficiency.html, (accessed 28 April 2020).

2 J. Burschka, N. Pellet, S. J. Moon, R. Humphry-Baker, P. Gao, M. K. Nazeeruddin and M. Grätzel, *Nature*, 2013, **499**, 316–319.

3 N. J. Jeon, J. H. Noh, W. S. Yang, Y. C. Kim, S. Ryu, J. Seo and

S. Il Seok, *Nature*, 2015, **517**, 476–480.
4 M. M. Lee, J. Teuscher, T. Miyasaka, T. N. Murakami and H. J. Snaith, *Science*, 2012, **338**, 643–647.
5 C. Wehrenfennig, G. E. Eperon, M. B. Johnston, H. J. Snaith and L. M. Herz, *Adv. Mater.*, 2014, **26**, 1584–1589.
6 M. Saliba, T. Matsui, J. Y. Seo, K. Domanski, J. P. Correa-Baena, M. K. Nazeeruddin, S. M. Zakeeruddin, W. Tress, A. Abate, A. Hagfeldt and M. Grätzel, *Energy Environ. Sci.*, 2016, **9**, 1989–1997.
7 M. A. Green, A. Ho-Baillie and H. J. Snaith, *Nat. Photonics*, 2014, **8**, 506–514.
8 B. Chen, Z. J. Yu, S. Manzoor, S. Wang, W. Weigand, Z. Yu, G. Yang, Z. Ni, X. Dai, Z. C. Holman and J. Huang, *Joule*, 2020, **4**, 850–864.
9 W. S. Yang, B. W. Park, E. H. Jung, N. J. Jeon, Y. C. Kim, D. U. Lee, S. S. Shin, J. Seo, E. K. Kim, J. H. Noh and S. Il Seok, *Science*, 2017, **356**, 1376–1379.
10 W. W. Liu, T. H. Wu, M. C. Liu, W. J. Niu and Y. L. Chueh, *Adv. Mater. Interfaces*, 2019, **6**, 1801758.
11 D. H. Kim, J. B. Whitaker, Z. Li, M. F. A. M. van Hest and K. Zhu, *Joule*, 2018, **2**, 1437–1451.
12 L. Qiu, L. K. Ono and Y. Qi, *Mater. Today Energy*, 2018, 7, 169–189.
13 Y. Rong, Y. Hu, A. Mei, H. Tan, M. I. Saidaminov, S. Il Seok, M. D. McGehee, E. H. Sargent and H. Han, *Science*, 2018, 361.
14 K. Rakstys, C. Igci and M. K. Nazeeruddin, *Chem. Sci.*, 2019, **10**, 6748–6769.
15 U. Bach, D. Lupo, P. Comte, J. E. Moser, F. Weissörtel, J. Salbeck, H. Spreitzer and M. Grätzel, *Nature*, 1998, **395**, 583–585.
16 W. S. Yang, J. H. Noh, N. J. Jeon, Y. C. Kim, S. Ryu, J. Seo and S. Il Seok, *Science*, 2015, **348**, 1234–1237.
17 G. W. Kim, H. Choi, M. Kim, J. Lee, S. Y. Son and T. Park, *Adv. Energy Mater.*, 2020, **10**, 1903403.
18 T. P. I. Saragi, T. Spehr, A. Siebert, T. Fuhrmann-Lieker and J. Salbeck, *Chem. Rev.*, 2007, **107**, 1011–1065.
19 J. Salbeck, F. Weissörtel and J. Bauer, *Macromol. Symp.*, 1998, **125**, 121–132.
20 J. Salbeck, N. Yu, J. Bauer, F. Weissörtel and H. Bestgen, *Synth. Met.*, 1997, **91**, 209–215.
21 B. Xu, D. Bi, Y. Hua, P. Liu, M. Cheng, M. Grätzel, L. Kloo, A. Hagfeldt and L. Sun, *Energy Environ. Sci.*, 2016, **9**, 873–877.
22 D. Bi, B. Xu, P. Gao, L. Sun, M. Grätzel and A. Hagfeldt, *Nano Energy*, 2016, **23**, 138–144.
23 B. Xu, J. Zhang, Y. Hua, P. Liu, L. Wang, C. Ruan, Y. Li, G. Boschloo, E. M. J. Johansson, L. Kloo, A. Hagfeldt, A. K. Y. Jen and L. Sun, *Chem*, 2017, **2**, 676–687.
24 T. Malinauskas, M. Saliba, T. Matsui, M. Daskeviciene, S. Urnikaite, P. Gratia, R. Send, H. Wonneberger, I. Bruder, M. Graetzel, V. Getautis and M. K. Nazeeruddin, *Energy Environ. Sci.*, 2016, **9**, 1681–1686.
25 K. Rakstys, S. Paek, G. Grancini, P. Gao, V. Jankauskas, A. M. Asiri and M. K. Nazeeruddin, *ChemSusChem*, 2017, **10**, 3825–3832.
26 A. Magomedov, S. Paek, P. Gratia, E. Kasparavicius, M. Daskeviciene, E. Kamarauskas, A. Gruodis, V. Jankauskas, K. Kantminiene, K. T. Cho, K. Rakstys, T. Malinauskas, V. Getautis and M. K. Nazeeruddin, *Adv. Funct. Mater.*, 2018, **28**, 1704351.
27 J. A. Christians, P. Schulz, J. S. Tinkham, T. H. Schloemer, S. P. Harvey, B. J. Tremolet De Villers, A. Sellinger, J. J. Berry and J. M. Luther, *Nat. Energy*, 2018, **3**, 68–74.
28 X. Li, M. Cai, Z. Zhou, K. Yun, F. Xie, Z. Lan, J. Hua and L. Han, *J. Mater. Chem. A*, 2017, **5**, 10480–10485.
29 L. Guan, X. Yin, D. Zhao, C. Wang, Q. An, J. Yu, N. Shrestha, C. R. Grice, R. A. Awni, Y. Yu, Z. Song, J. Zhou, W. Meng, F. Zhang, R. J. Ellingson, J. Wang, W. Tang and Y. Yan, *J. Mater. Chem. A*, 2017, **5**, 23319–23327.
30 F. Wu, Y. Shan, J. Qiao, C. Zhong, R. Wang, Q. Song and L. Zhu, *ChemSusChem*, 2017, **10**, 3833–3838.
31 C. Lu, I. T. Choi, J. Kim and H. K. Kim, *J. Mater. Chem. A*, 2017, **5**, 20263–20276.
32 R. Xue, M. Zhang, G. Xu, J. Zhang, W. Chen, H. Chen, M. Yang, C. Cui, Y. Y. Li and Y. Y. Li, *J. Mater. Chem. A*, 2018, **6**, 404–413.
33 J. Zhang, Y. Hua, B. Xu, L. Yang, P. Liu, M. B. Johansson, N. Vlachopoulos, L. Kloo, G. Boschloo, E. M. J. Johansson, L. Sun and A. Hagfeldt, *Adv. Energy Mater.*, 2016, **6**, 1601062.
34 D. Li, J. Y. Shao, Y. Y. Li, Y. Y. Li, L. Y. Deng, Y. W. Zhong and Q. Meng, *Chem. Commun.*, 2018, **54**, 1651–1654.
35 B. Bin Cui, C. Zhu, S. Yang, Y. Han, N. Yang, L. Zhang, Y. Wang, Y. Jia, L. Zhao and Q. Chen, *ACS Omega*, 2018, **3**, 10791–10797.
36 K. Rakstys, M. Saliba, P. Gao, P. Gratia, E. Kamarauskas, S. Paek, V. Jankauskas and M. K. Nazeeruddin, *Angew. Chemie - Int. Ed.*, 2016, **55**, 7464–7468.
37 F. Zhang, Z. Wang, H. Zhu, N. Pellet, J. Luo, C. Yi, X. Liu, H. Liu, S. Wang, X. Li, Y. Xiao, S. M. Zakeeruddin, D. Bi and M. Grätzel, *Nano Energy*, 2017, **41**, 469–475.
38 F. Zhang, S. Wang, H. Zhu, X. Liu, H. Liu, X. Li, Y. Xiao and S. M. Zakeeruddin, *ACS Energy Lett.*, 2018, **3**, 1145–1152.
39 M. L. Petrus, A. Music, A. C. Closs, J. C. Bijleveld, M. T. Sirtl, Y. Hu, T. J. Dingemans, T. Bein and P. Docampo, *J. Mater. Chem. A*, 2017, **5**, 25200–25210.
40 M. L. Petrus, M. T. Sirtl, A. C. Closs, T. Bein and P. Docampo, *Mol. Syst. Des. Eng.*, 2018, **3**, 734–740.
41 M. L. Petrus, K. Schutt, M. T. Sirtl, E. M. Hutter, A. C. Closs, J. M. Ball, J. C. Bijleveld, A. Petrozza, T. Bein, T. J. Dingemans, T. J. Savenije, H. Snaith and P. Docampo, *Adv. Energy Mater.*, 2018, **8**, 1–11.
42 D. Vaitukaityte, Z. Wang, T. Malinauskas, A. Magomedov, G. Bubniene, V. Jankauskas, V. Getautis and H. J. Snaith, *Adv. Mater.*, 2018, **30**, 1–7.
43 M. Daskeviciene, S. Paek, Z. Wang, T. Malinauskas, G. Jokubauskaite, K. Rakstys, K. T. Cho, A. Magomedov, V. Jankauskas, S. Ahmad, H. J. Snaith, V. Getautis and M. K. Nazeeruddin, *Nano Energy*, 2017, **32**, 551–557.
44 M. Daskeviciene, S. Paek, A. Magomedov, K. T. Cho, M. Saliba, A. Kizeleviciute, T. Malinauskas, A. Gruodis, V. Jankauskas, E. Kamarauskas, M. K. Nazeeruddin and V. Getautis, *J. Mater. Chem. C*, 2019, **7**, 2717–2724.
45 T. P. Osedach, T. L. Andrew and V. Bulović, *Energy Environ. Sci.*, 2013, **6**, 711–718.

46 M. L. Petrus, T. Bein, T. J. Dingemans and P. Docampo, *J. Mater. Chem. A*, 2015, **3**, 12159–12162.

47 A. C. Recommendations, Gaussian 09 Citation | Gaussian.com, https://gaussian.com/g09citation/, (accessed 15 May 2020).

48 J. Urieta-Mora, I. García-Benito, I. Zimmermann, J. Aragó, J. Calbo, G. Grancini, A. Molina-Ontoria, E. Ortí, N. Martín and M. K. Nazeeruddin, *J. Mater. Chem. C*, 2019, **7**, 6656–6663.

49 K. Walzer, B. Männig, M. Pfeiffer and K. Leo, *Chem. Rev.*, 2007, **107**, 1233–1271.

50 B. Lüssem, M. Riede and K. Leo, *Phys. Status Solidi Appl. Mater. Sci.*, 2013, **210**, 9–43.

51 I. Salzmann, G. Heimel, M. Oehzelt, S. Winkler and N. Koch, *Acc. Chem. Res.*, 2016, **49**, 370–378.

52 J. Y. Feng, K. W. Lai, Y. S. Shiue, A. Singh, C. H. P. Kumar, C. T. Li, W. T. Wu, J. T. Lin, C. W. Chu, C. C. Chang and C. C. Su, *J. Mater. Chem. A*, 2019, **7**, 14209–14221.

53 Y. Lee, S. Paek, K. T. Cho, E. Oveisi, P. Gao, S. Lee, J. S. Park, Y. Zhang, R. Humphry-Baker, A. M. Asiri and M. K. Nazeeruddin, *J. Mater. Chem. A*, 2017, **5**, 12729–12734.

54 K. Rakstys, A. Abate, M. I. Dar, P. Gao, V. Jankauskas, G. Jacopin, E. Kamarauskas, S. Kazim, S. Ahmad, M. Grätzel and M. K. Nazeeruddin, *J. Am. Chem. Soc.*, 2015, **137**, 16172–16178.

55 D. Shi, X. Qin, Y. Li, Y. He, C. Zhong, J. Pan, H. Dong, W. Xu, T. Li, W. Hu, J. L. Brédas and O. M. Bakr, *Sci. Adv.*, 2016, **2**, e1501491.

56 M. Namatame, M. Yabusaki, T. Watanabe, Y. Ogomi, S. Hayase and K. Marumoto, *Appl. Phys. Lett.*, 2017, **110**, 123904.

57 N. Drigo, C. Roldan-Carmona, M. Franckevičius, K. H. Lin, R. Gegevičius, H. Kim, P. A. Schouwink, A. A. Sutanto, S. Olthof, M. Sohail, K. Meerholz, V. Gulbinas, C. Corminboeuf, S. Paek and M. K. Nazeeruddin, *J. Am. Chem. Soc.*, 2020, **142**, 1792–1800.

58 G. Xing, N. Mathews, S. Sun, S. S. Lim, Y. M. Lam, M. Graẗzel, S. Mhaisalkar and T. C. Sum, *Science*, 2013, **342**, 344–347.

59 T. Braukyla, R. Xia, T. Malinauskas, M. Daskeviciene, A. Magomedov, E. Kamarauskas, V. Jankauskas, Z. Fei, C. Roldán-Carmona, C. Momblona, M. K. Nazeeruddin, P. J. Dyson and V. Getautis, *Sol. RRL*, 2019, **3**, 1900224.

60 A. Magomedov, E. Kasparavičius, K. Rakstys, S. Paek, N. Gasilova, K. Genevičius, G. Juška, T. Malinauskas, M. K. Nazeeruddin and V. Getautis, *J. Mater. Chem. C*, 2018, **6**, 8874–8878.

61 E. Kasparavicius, A. Magomedov, T. Malinauskas and V. Getautis, *Chem. - A Eur. J.*, 2018, **24**, 9910–9918.

62 A. K. Jena, M. Ikegami and T. Miyasaka, *ACS Energy Lett.*, 2017, 2, 1760–1761.

63 J. Zhang, Q. Daniel, T. Zhang, X. Wen, B. Xu, L. Sun, U. Bach and Y. B. Cheng, *ACS Nano*, , DOI:10.1021/acsnano.8b06062.